钼对钴基合金激光熔覆层组织与耐磨性的影响

李明喜，　修俊杰，　赵庆宇，　何宜柱
（安徽工业大学 材料科学与工程学院，安徽 马鞍山　243002）

摘　要：利用激光熔覆技术在低碳钢基体表面制备了钴基合金涂层. 利用金相显微镜(OP)、扫描电镜(SEM)及 X 射线衍射仪(XRD)等研究了不同 Mo 元素含量的钴基合金涂层的组织结构；通过采用显微硬度试验、滑动磨损试验等方法进行性能测试. 结果表明，含 5.4%Mo 的合金熔覆层主要组成相为 γ-Co，$Cr_{23}C_6$，而含 28%Mo 的合金涂层主要相组成为 γ-Co，$Cr_{23}C_6$，Co_3Mo_2Si 和 NiCoCr 等相；含 5.4%Mo 涂层的组织主要为柱状生长树枝晶；含 28% Mo 单道涂层的结合区为紊乱的粗大树枝晶，中部为向上生长的细小的树枝晶，表层为细小的等轴晶，多道搭接涂层组织为细小的等轴晶；含 28%Mo 涂层的显微硬度可达 800 HV 以上，比含 5.4%Mo 涂层的硬度提高了一倍；耐磨性也有不同程度的提高.

关键词：激光熔覆；钴基合金；钼；组织
中图分类号：TG146.2　　文献标识码：A　　文章编号：0253－360X(2009)11－0017－04

李明喜

0　序　　言

激光熔覆是金属表面改性的一种有效手段. 激光熔覆具有快速熔化、快速凝固的特点，可在普通金属材料表面制取高性能的涂层[1－4]. 钴基合金激光熔覆层具有良好的高温性能，但其室温硬度却较低[5－8]. 钼是钴基合金粉末中常用的成分之一，但一般含量较低，为进一步提高涂层的室温硬度和耐磨性，可增加其含量. 因此，文中研究了加入不同 Mo 元素含量的钴基合金激光熔覆层，探讨钼对熔覆层组织和耐磨性的影响规律.

1　试验方法

基体材料为 SPHC 钢，尺寸为 100 mm×80 mm×8 mm. 熔覆材料选用钴基合金与钼粉. 钴基合金粉末粒度为 53～120 μm. 基体及合金材料见表 1 和表 2.

表 1　SPHC 钢化学成分(质量分数，%)

Table 1　Chemical compositions of SPHC steel

C	Mn	Si	P	S	Fe
0.050	0.220	0.020	0.015	0.010	余量

表 2　钴基合金粉末化学成分(质量分数，%)

Table 2　Chemical composition of Co-based alloy

	C	Cr	Mo	Ni	Si	Fe	Co
合金 A	0.27	28.60	5.40	2.27	0.90	0.50	余量
合金 B	0.21	21.77	28.00	1.73	0.69	0.38	余量

熔覆前将 SPHC 钢基材表面除锈磨平，在钴基合金粉末中添加纯度为 99.9%钼粉，粒度为 2.5～3.5 μm，在研磨钵中充分混合均匀. 熔覆前将基材和合金粉末在 120 ℃条件下烘干 3 h. 因不同粉末密度不同，同步送粉会出现不均匀，故采用预置粉末法，预置合金粉末厚度约 1.0 mm. 采用 TJ－HL－5000 横流 CO_2 连续激光器进行激光熔覆处理，工艺参数为输出功率 2.3 kW，光斑直径 5.0 mm，多道搭接率为 50%，扫描速度分别为 160，240 mm/min，熔覆过程中以氩气作为保护气体.

用 Olympus Pme－3 型金相显微镜及 Philip－Xl 30 型扫描电镜观察组织及拍照；用 XD－3A 衍射仪分析熔覆层的相组成；用 MM－200 环—块滑动试验机测定涂层的耐磨性；对磨材料为模具钢表面激光熔覆 WC_P/Ni 基涂层，硬度为 65 HRC，其外径为 40 mm，内径为 10 mm，厚度为 10 mm，载荷为 30 N，试验机转速为 200 r/min，用 1∶100 乳化液冷却，用感量为 0.000 1 g 的分析天平称重. 每个试样先预磨 3 min，清洗称重后再正式试验，每磨损 10 min 清洗称重一次，总磨损时间为 60 min.

收稿日期：2008－07－28
基金项目：安徽省国际科技合作项目资助计划(08080703020)；安徽省教育厅自然科学研究资助项目(KJ2007A106ZC)

2 试验结果及分析

2.1 相组成分析

图 1 为两种熔覆层的 XRD 衍射图谱. 从图 1a 可以看出, 合金 A 涂层主要由 γ-Co, $Cr_{23}C_6$ 相组成. 与合金 A 涂层相比, 合金 B 涂层增加了 Co_3Mo_2Si[9] 和 NiCoCr 两种新相, 见图 1b.

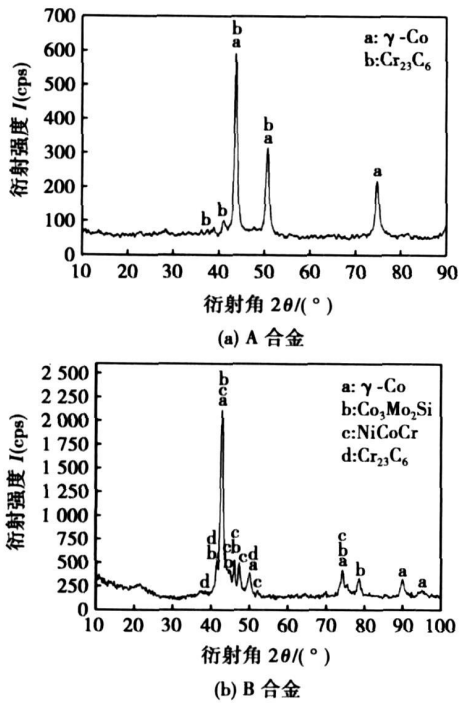

图 1 熔覆层的 X 射线衍射图谱

Fig. 1 XRD Pattern of coatings

由图 1 可见, 合金 B 涂层的相结构仍以 γ-Co 固溶体为主; Mo, Cr 两种元素都是封闭 ε 区、扩大 α 区元素, 且两种元素在涂层中的含量都超过 20%, 涂层未出现 ε-Co. 显然, 激光熔覆快速冷却作用使 γ-Co 来不及向 ε-Co 转变.

2.2 激光熔覆层的显微组织观察及分析

图 2 为两种合金在不同扫描速度下单道涂层的低倍金相组织. 在扫描速度为 200 mm/min 时, 含 5.4%Mo 的合金 A 涂层的界面区组织大致垂直于界面的树枝晶, 见图 2a. 含 28%Mo 的合金 B 涂层的界面区组织已发生明显的变化, 为不明显的、方向紊乱的组织, 中部为向上生长的细小的树枝晶, 见图 2b; 在扫描速度为 160 mm/min 时, 合金 B 涂层中部为多方向生长的细小的树枝晶, 见图 2c; 表层为细小的等轴晶组织, 见图 2d.

图 3 为合金 B 在扫描速度为 240 mm/min 时, 多

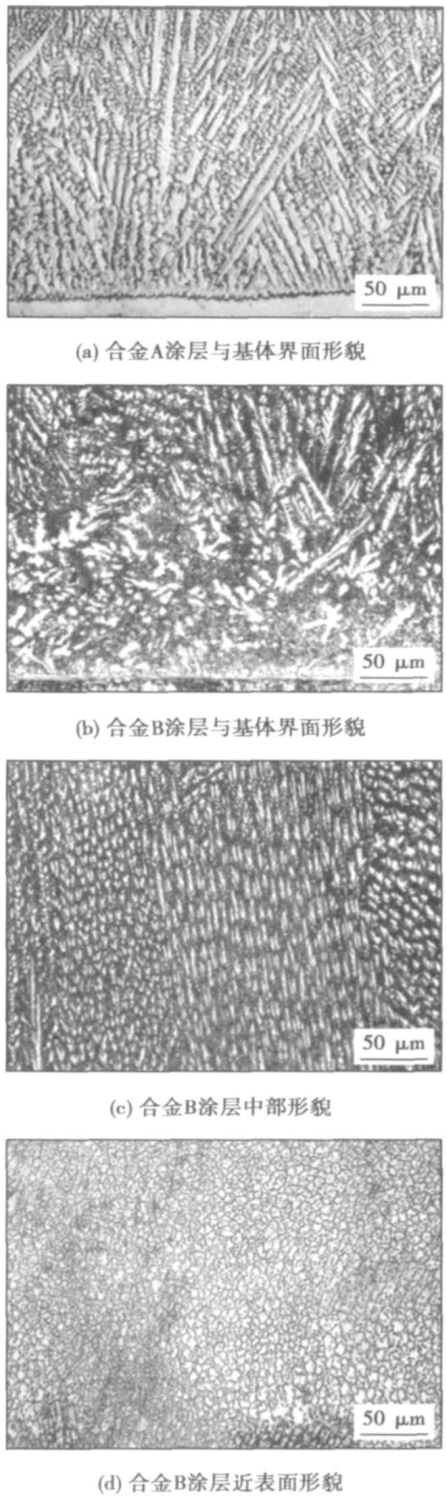

图 2 熔覆层的金相组织形貌

Fig. 2 Microstructure of laser coatings

道搭接熔覆层组织形貌, 与单道涂层组织(图 2b)相比, 已发生明显的变化: 定向凝固典型的枝晶组织特征基本消失, 取而代之的是除搭接区有部分枝晶形态外的等轴晶组织, 见图 3a. 熔覆层的中下部为拉长的等轴晶形态, 见图 3b. 对涂层组织中的晶内及晶界微区成分分析结果, 如表 3 所示. 从表 3 可以

看出，A 区应为固溶了大量 Mo，Cr 和 Fe 元素的 γ-Co 固溶体；晶间为 γ-Co 与 Co_3Mo_2Si 的共晶组织或 γ-Co 与 $Cr_{23}C_6$ 的共晶组织．从 Si 元素含量的不同来看，Co_3Mo_2Si 这种 Laves 相主要弥散分布在 γ-Co 基体中．

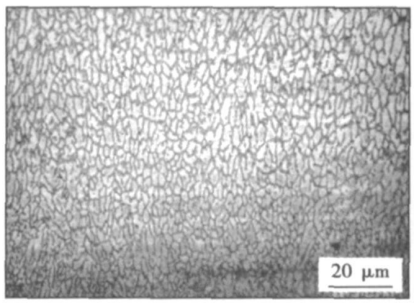

(a) 涂层近表面形貌

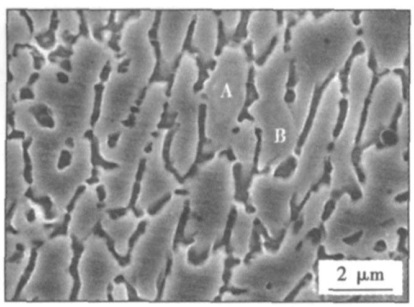

(b) 涂层中部形貌

图 3　合金 B 多道搭接涂层的微观组织形貌

Fig. 3　Microstructure of multi-track coatings for alloy B

表 3　图 3b 中微区成分分析结果(质量分数，%)

Table 3　Energy spectrum analysis of marked areas in Fig. 3b

	Co	Cr	Mo	Ni	Fe	Si
A 区	44.51	18.87	25.55	2.77	7.61	0.70
B 区	46.17	19.65	23.58	2.72	7.66	0.22

激光熔池凝固以非均匀形核为主，形核的场所主要有两种，一是熔池中的未熔悬浮质点，比如一些难熔的金属元素；二是熔池底部未熔化的基材表面．添加的钼熔点高达 2 620 ℃，而且含量占到 28%，如此多细小的、高熔点的钼颗粒可作为熔池中的未熔悬浮质点而成为异质形核的现成表面，增加形核率；另外，熔池中反应生成的高熔点的 Co_3Mo_2Si 等金属间化合物也可能作为异质形核的核心，进一步增加形核率．

粉末吸收率增加，基材温度场的变化导致固液界面前沿温度梯度 G 变小、成分过冷区域变大，高熔点的钼增加了形核率，这些都对得到等轴晶有利．

2.3　熔覆层的显微硬度及耐磨性测试结果

图 4 为熔覆层的硬度和耐磨性试验结果．图 4a 为熔覆层的显微硬度分布，从图中可见，Mo 元素含量为 5.4%的 A 合金，涂层的平均硬度约为 400 HV；Mo 元素含量为 28%的 B 合金，硬度可达 800 HV 以上，并且当扫描速度大(240 mm/s)时，涂层的硬度更高(平均约为 850 HV)．

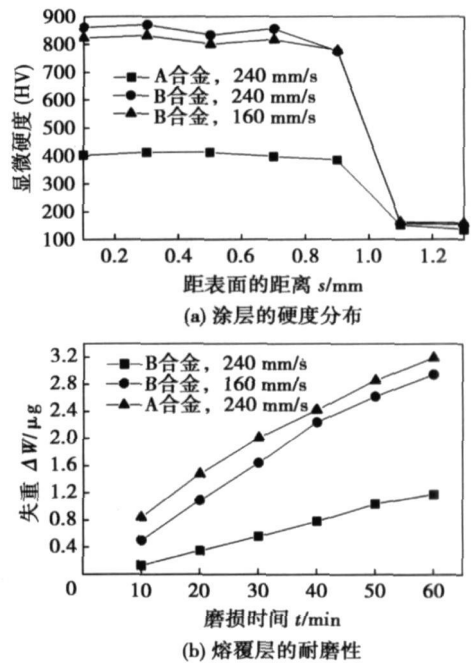

图 4　熔覆层的显微硬度和耐磨性

Fig. 4　Microhardness and wear-resistance of coatings

合金 B 混合粉末中含有大量的 Cr，Mo(> 20%)元素和少量的 Si，C 等合金元素，在激光的高温作用下极易形成硬质相而提高涂层的硬度．碳对提高熔覆层的硬度作用很大，一方面可以固溶到涂层中，产生固溶强化；另一方面可以与强碳化物元素 Cr 等反应生成高硬度的碳化物．一般情况下，钼以固溶强化作用来影响涂层的硬度；但当 Mo 元素含量很高且有 Si 元素的情况下，也能在熔池中发生如下反应，即

$$Co + Mo + Si \rightarrow Co_3Mo_2Si$$

XRD 物相分析已确定，合金 B 涂层中存在这种脆硬的 Laves 相．另外合金 B 涂层中还有其它金属间化合物．这些硬质相弥散分布在细小的等轴晶内，对涂层起到了显著的弥散强化作用．总之，第二相对涂层的弥散强化、合金元素在涂层中的固溶强化及涂层组织的细化等综合作用，使合金 B 涂层的硬度大大提高．

图 5 为熔覆层(扫描速度为 160 mm/min)的滑动

磨痕形貌. 当对磨环与合金 A 涂层相互对磨时, 由于合金 A 涂层硬度较低, 对磨环上凸起的硬质颗粒很容易嵌入其中. 犁削过程中即使遇到较硬的碳化物, 犁削也不易中止, 因此导致涂层磨损失重较大, 形成的犁沟较深、较大, 见图 5a. 合金 B 涂层由于硬度高, 抵抗磨削应力的能力强, 因而磨损失重较小, 磨痕细小, 见图 5b.

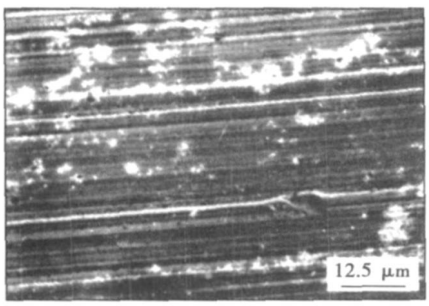

(a) A合金

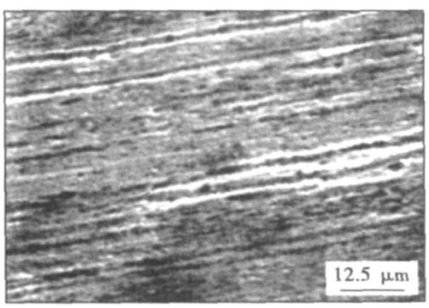

(b) B合金

图 5 熔覆层的磨损形貌

Fig. 5 Worn surface of coatings

3 结 论

(1) 合金 A 熔覆层主要组成相为 γ-Co, $Cr_{23}C_6$; 合金 B 涂层主要相组成为 γ-Co, $Cr_{23}C_6$, Co_3Mo_2Si 和 NiCoCr 等相.

(2) 合金 A 涂层的组织主要为柱状生长的树枝晶; 合金B单道涂层的结合区为紊乱的粗大树枝晶, 中部为向上生长的细小的树枝晶, 表层为细小的等轴晶; 而合金 B 的多道搭接组织为细小的等轴晶.

(3) 合金 B 涂层的硬度可达 800 HV 以上, 比合金 A 涂层的硬度提高一倍, 耐磨性也有所提高.

参考文献:

[1] Liu Y, Wang H M. Elevated temperature wear behaviors of a Co-Mo-Si ternary metal silicide alloy[J]. Scripta Materialia, 2005, 52(12): 1235—1240.

[2] Lin W C, Chen C. Characteristics of thin surface layers of cobalt-based alloys deposited by laser cladding[J]. Surface and Coatings Technology, 2006, 200(14—15): 4557—4563.

[3] Sun S, Brandt M, Harris J, *et al*. The influence of stellite 6 particle size on the inter-track porosity in multi-track cladding[J]. Surface and Coatings Technology, 2006, 201(3—4): 998—1005.

[4] Navas C, Cadenas M, Cuetos J M, *et al*. Microstructure and sliding wear behaviour of Tribaloy T-800 coatings deposited by laser cladding [J]. Wear, 2006, 206(7—8): 838—846.

[5] Ocelik V, Oliveira de U, Boer de M, *et al*. Thick Co-based coating on cast iron by side laser cladding: Analysis of processing conditions and coating properties[J]. Surface and Coatings Technology, 2007, 201(12): 5875—5883.

[6] Li Mingxi, He Yizhu, Sun Guoxiong. Microstructure and wear resistance of laser clad cobalt-based alloy mutilayer coatings[J]. Applied Surface Science, 2004, 230(1—4): 201—206.

[7] Cui Chengyun, Guo Zuoxing, Liu Yuhua, *et al*. Characteristics of cobalt-based alloy coating on tool steel prepared by powder feeding laser cladding[J]. Optics & Laser Technology, 2007, 39(8): 1544—1550.

[8] Graça S, Colaço R, Vilar R. Indentation size effect in nickel and cobalt laser clad coatings[J]. Surface and Coatings Technology, 2007, 202(3): 538—548.

[9] Przybylowicz J, Kusinski J. Laser cladding and erosive wear of Co-Mo-Cr-Si coatings[J]. Surface and Coatings Technology, 2000, 125(1—3): 13—18.

作者简介: 李明喜, 男, 1966 年出生, 博士, 教授. 主要从事激光表面工程的基础研究与应用. 发表论文 40 余篇.

Email: limingxi @ahut. edu. cn

proved by lower elastic modulus adhesive and the center overlapping of the nugget and the lap zone.

Key words: adhesive-welded joint; elastic modulus; double lap joint; stress distribution; numerical analysis

Effect of Mo content on microstructure and wear resistance of Co-based coatings by laser cladding LI Mingxi, XIU Junjie, ZHAO Qingyu, HE Yizhu (School of Materials Science and Engineering, Anhui University of Technology, Maanshan 243002, Anhui, China). p 17—20

Abstract: Co-based alloy coatings with different Mo content (5.4% and 28%) on the surface of low carbon steel were prepared by laser cladding. The microstructure and phases composition of the coatings were investigated by means of optical microscope (OP), scanning electron microscope (SEM) and X-ray diffraction instrument (XRD). Microhardness and sliding wear resistance of the coatings were also tested. The results indicated that the main phases in Co-based alloy coatings with 5.4% Mo were γ-Co and $Cr_{23}C_6$. Another two phases of Co_3Mo_2Si and NiCoCr were identified in Co-based alloy coatings with 28% Mo. Directional dendrite was observed in Co-based alloy coatings with 5.4% Mo. Unidirectional dendrite at the interface, followed by fine dendrite at the central zone and equiaxed grain near top surface were found in Co-based alloy single coatings with 28% Mo, and almost all fine equiaxed grains appear in the multi-track coatings. The microhardness of Co-based alloy coatings with 28% Mo reaches up to 800 HV, which was 2 times of that of Co-based alloy coatings with 5.4% Mo. The sliding wear resistance was also improved.

Key words: laser cladding; Co-based alloy; molybdenum; microstructure

Laser aided activating TIG welding ZHANG Ruihua[1], YIN Yan[1], Mizitani[2], Katayama[2] (1. State Key Laboratory of Gansu Advanced Non-ferrous Metal Materials, Lanzhou University of Technology, Lanzhou 730050, China; 2. JWRI, Osaka University, Osaka 567-0047, Japan). p 21—24

Abstract: On the bases of the study for the mechanism of the increasing of A-TIG welding penetration, a new method of activating TIG welding, the laser aided activating TIG welding was proposed. At first, the surface of weld was melt by the mini power laser protected by oxygen. As a result, the oxygen content increases in the weld pool surface. Then the conventional TIG welding was used to cover the weld. The oxygen could change the direction of fluid flow in molten pool, which leads to the weld beads with narrower width and deeper penetration. Without the activating flux, the penetration can be increased by 2 times. There is no slag in the surface of weld and the appearance is good. The oxygen can change the temperature dependence of surface tension gradient from a negative value to a positive value; and cause the significant changes in the weld penetration. Fluid flow could be inward along the surface of the weld pool toward the center and then down. This fluid flow pattern transfers heat to the weld root and produces a relatively deep and narrow weld efficiently. This change is the main cause to increase the penetration.

Key words: activating TIG welding; laser; penetration increase

Analysis of different welding conditions on variable polarity plasma arc pressure JIANG Yi, XU Binshi, LÜ Yaohui, LIU Cunlong (National Key Laboratory for Remanufacturing, Academy of Armored Forces Engineering, Beijing 100072, China). p 25—28

Abstract: VPPA pressure was measured at different welding parameters by U-tube barometer method. The effects of different welding conditions on arc force, including straight polarity current, reverse polarity current, time ratio, plasma gas flow rate were analyzed by the orthogonal experiment. The results indicates that VPPA pressure increased with these four parameters, and the influences of the welding parameters are in order of plasma gas flow rate, straight polarity current, time ratio, and reverse polarity current. Then the mechanisms were discussed. The plasma gas can cool and compress the arc column and compress the arc radius, which increases the VPPA pressure; while the welding current increases the arc radius by electromagnetic compression, which enhances the VPPA pressure. Moreover, due to the great difference of VPPA pressure between straight polarity phase and reverse polarity phase, time ratio is also one of key factors to VPPA pressure.

Key words: variable polarity plasma arc welding; arc force; U-tube barometer; orthogonal experiment

Characteristic of energy distribution at anode and cathode on AC TIG welding arc YANG Xiaohong, SONG Yonglun, HU Kunping, XIA Yuan (College of Mechanical Engineering & Applied Electronics Technology, Beijing University of Technology, Beijing 100124, China). p 29—32

Abstract: During AC TIG welding of aluminum alloy, the physical phenomena of welding arc plasma at electrode negative (EN) and electrode positive (EP) periods and the characteristic of energy distribution at anode and cathode were investigated by observing the spectrum and founding the mathematical models. Furthermore, cathodic cleaning effect increases with the percentage of electrode positive. The dependence of electron density on time in the whole cycle is obtained with the theory of spectral line Stark broadening and the characteristic of energy distribution is analyzed through the mathematical models. The mechanism of emitting electrons, cathodic cleaning and the quality of weld is better understood by observing the spectrum of argon, aluminum and oxygen respectively during EN and EP periods.

Key words: AC TIG welding arc; dynamic spectroscopic diagnostic; electron density; energy distribution

Fiber laser-MIG hybrid welding process of commercial pure titanium and its properties CUI Li[1], LI Xiaoyan[1], HE Dingyong[1], KUTSUNA Muneharu[2] (1. College of Materials Science and Engineering, Beijing University of Technology, Beijing 100124, China; 2. Nagoya University, Nagoya 464-8603, Japan). p 33—36

Abstract: Fiber laser-metal inert gas (MIG) arc hybrid welding was used to weld the commercial pure titanium (CP-Ti). The weld appearance, cross section, tensile strength, Erichsen value and microstructure of the CP-Ti welded joints were studied. The results show that the arc stability is substantially improved and the welding speed can be increased to 7 times by fiber laser-MIG hybrid welding. The welded joints by laser welding and the hybrid welding exhibit the higher ultimate tensile strength than those of the base